Myosin II Heavy Chain Null Mutant of *Dictyostelium* Exhibits Defective Intracellular Particle Movement

Deborah Wessels and David R. Soll

Department of Biology, University of Iowa, Iowa City, Iowa 52242

Abstract. Both cellular motility and intracellular particle movement are compared between normal *Dictyostelium* amebae of strain AX4 and amebae of a myosin II heavy chain null mutant, HS2215, using the computer assisted "Dynamic Morphology System." In AX4 cells rapidly translocating in buffer, cytoplasmic expansion is apical and the majority of intracellular particles move anteriorly, towards the site of expansion. When these cells are pulsed with 10^{-6} M cAMP, the peak concentration of the natural cAMP wave, cells stop translocating and average particle velocity decreases threefold within 2–4 s after cAMP addition. After 8 s, there is a partial rebound both in cytoplasmic expansion and particle velocity, but in both cases, original apical polarity is lost. In HS2215 cells in buffer, both cellular translocation and average particle velocity are already at the depressed levels observed in normal cells immediately after cAMP addition, and no anterior bias is observed in either the direction of cytoplasmic expansion or the direction of particle movement. The addition of cAMP to myosin-minus cells results in no additional effect. The results demonstrate that myosin II is necessary for (*a*) the rapid rate of intracellular particle movement, (*b*) the biased anterior directionality of particle movement, and (*c*) the rapid inhibition of particle movement by cAMP.

RECENTLY, the function of myosin II was investigated in *Dictyostelium discoideum* by generating cells deficient in myosin II heavy chain either by antisense RNA inactivation (Knecht and Loomis, 1987) or by disruption of the myosin heavy chain gene through homologous recombination (De Lozanne and Spudich, 1987). The phenotypes of the two myosin-deficient cell lines were similarly defective. Myosin-deficient cells exhibited defective cytokinesis, but were capable of cell movement, phagocytosis, and chemotactic behavior (De Lozanne and Spudich, 1987; Knecht and Loomis, 1987; Peters et al., 1988; Wessels et al., 1988). Although myosin-deficient cells were capable of movement, the manner in which they translocated was aberrant (Wessels et al., 1988). Myosin-deficient cells moved at rates of translocation less than half that of normal cells. They were rounder and less polar, forming expansion zones randomly around the cell perimeter rather than in a polarized fashion in an apical zone. Finally, the speed and shape of expansion zones formed by the myosin-deficient strains differed from those formed in the anterior region of rapidly translocating normal cells. These results, in combination with experiments demonstrating that antibodies to myosin II injected into *Acanthamoeba* slow but do not stop locomotion (Sinard and Pollard, 1989), suggested that myosin II was indeed necessary for normal amebic motility.

Myosin II has been demonstrated to be present in the cortex of the posterior two-thirds of aggregation-competent *Dictyostelium* amebae flattened by agarose overlays, but at either negligible or very low levels in anterior pseudopodial regions (Fukui and Yumura, 1986). This localization pattern has been interpreted to suggest that a myosin-based mechanism is involved in posterior cortical contraction in ameboid movement (Fukui and Yumura, 1986; Spudich, 1989). In addition, myosin II has been demonstrated by electron microscopic localization with IgG–gold conjugates to be associated with small cytoplasmic vesicles in *Dictyostelium* Ogihara et al., 1988), suggesting an additional role in intracellular organelle movement.

By using DIC optics, the computer-assisted "Dynamic Morphology System" (DMS)[1] (Soll, 1988; Soll et al., 1987, 1988), and a new system for analyzing intracellular particle motility (Wessels et al., 1989), we have examined both cellular and intracellular particle movement before and after the addition of cAMP in normal *D. discoideum* AX4 amebae and in amebae of a myosin heavy chain null mutant, HS2215 (formerly mhcA$^-$/A5), derived from strain AX4 (Manstein et al., 1989). The results demonstrate that myosin II is necessary for (*a*) rapid and apically directed intracellular particle movement, (*b*) rapid, polarized cellular translocation, and (*c*) rapid inhibition of particle movement by cAMP.

Materials and Methods

Maintenance of Stock Cultures

Stock cultures of the parent strain AX4 and the myosin heavy chain null

1. *Abbreviation used in this paper*: DMS, Dynamic Morphology System.

© The Rockefeller University Press, 0021-9525/90/09/1137/12 $2.00

mutant HS2215 (Manstein et al., 1989) were stored at −70°C. Both parent and mutant strains were generous gifts from Dr. J. Spudich, Stanford University, CA. Cell growth was initiated in 15-cm petri dishes containing 20 ml of the nutrient medium HL5 (Cocucci and Sussman, 1970) plus 10 μg/ml of G418 according to the methods of De Lozanne and Spudich (1987).

Generating Aggregation-competent Amebae

Development was initiated according to methods previously described (Soll, 1987; Wessels et al., 1988). In brief, cells in the midlog phase of growth were washed free of nutrient medium and dispersed on development pads saturated with buffered salt solution. Cultures were incubated at 22°C in a humidity chamber. Cells were harvested for experimental purposes at the onset of aggregation, when, in the case of normal cells, they have been demonstrated to exhibit maximum motility and responsiveness to cAMP (Varnum and Soll, 1984). In the case of AX4 cells, the onset of aggregation was 7 h, and in the case of HS2215 cells, it was 9 h.

Monitoring Cellular Behavior and Intracellular Particle Movement

The methods for harvesting cells, inoculating cells into a perfusion chamber, and treating with cAMP were identical to those described in a preceding publication (Wessels et al., 1989). In brief, 0.3 ml of cells at a density of 3×10^4 per ml was inoculated into a Dvorak-Stotler chamber (Nicholson Precision Instruments Inc., Gaithersburg, MD). The chamber was placed on the stage of a Zeiss ICM405 inverted microscope equipped with DIC optics. The chamber was perfused with buffered salts solution so that the chamber fluid was replaced every 7.7 s. After perfusion with buffered salts solution, cells were perfused with the same solution containing 10^{-6} M cAMP. The time at which cAMP first entered the chamber region containing the cell being monitored was estimated with a certainty of ± 1 s, and the time it took to achieve maximum cAMP concentration was 8 s (Wessels et al., 1989).

Cellular behavior was recorded on 3/4-in tape with a Sony U-Matic VO-5800 and analyzed either qualitatively by simply examining cellular and intracellular particle behavior on a monitor screen, or quantitatively with the DMS according to methods previously described (Soll, 1988; Soll et al., 1987, 1988). In the DMS system, the x,y coordinates of the pixels at the edge of selected cells were digitally recorded as frequently as every frame, and used to calculate centroid positions. "Instantaneous velocity" of centroid translocation was calculated for a cell in a given frame (n) by drawing a vector from the centroid in the previous frame ($n - 1$) to the centroid in the subsequent frame ($n + 1$), and the length of the vector divided by $2\Delta t$, where Δt is the time interval between frames. Difference pictures were produced by superimposing cell outlines of consecutive frames with 4-s intervals. Areas of expansion were filled, areas of contraction were hatched, and areas in common were left unfilled.

Intracellular particle movement was analyzed in the same cells analyzed for whole cell behavior. The methods were those described in a previous publication (Wessels et al., 1989). Particle positions were entered into the Dynamic Morphology System using the SVUI Manual Digitizer (SVUI, Iowa City, Iowa) with a program compensating for distortion. Particle positions were recorded every 0.5 s. Instantaneous particle velocity was calculated in the same manner as instantaneous centroid velocity. The mean direction vector for each particle was computed to be

$$V = V_1 + V_2 + \ldots + V_n,$$

where V_i is the central difference velocity vector for the particle at frame i and

$$V_1 = (x_2 - x_1,\ y_2 - y_1)/\Delta t,$$
$$V_i = (x_{i+1} - x_{i-1},\ y_{i+1} - y_{i-1})/2\Delta t \text{ where } 1 < i < n, \text{ and}$$
$$V_n = (x_n - x_{n-1},\ y_n - y_{n-1})/\Delta t.$$

In this case, n is the total number of frames, (x_i, y_i) is the position of the particle at frame i and Δt is the time interval between frames, in this case 0.5 s. To graphically illustrate particle directionality in relation to the direction of cellular translocation, the average direction of the particle (0–180°) was defined as the angle between V and the vector representing the average direction of centroid translocation during the 10-s period before cAMP addition. For example, if V was exactly in the direction of average centroid translocation, the average direction of the vesicle would be 0°. If V was directly opposite the direction of average centroid translocation, the average direction of the vesicle would be 180°.

Analysis of Particle Direction

The standard deviation of vector direction (SD) was computed as follows: each vector in a standard x,y Cartesian coordinate system, (x_i, y_i) ($i = 1, \ldots, n$) was converted to its unit vector $(\hat{x}_i, \hat{y}_i)$ by the formulas:

$$\hat{x}_i = x_i/\sqrt{x_i^2 + y_i^2},\ y_i = \hat{y}_i/\sqrt{x_i^2 + y_i^2}.$$

Then, the mean and standard deviations were computed for $\hat{x}_i$ and $\hat{y}_i$ separately to give means $m_{\hat{x}}$, $m_{\hat{y}}$ and standard deviations $S_{\hat{x}}$, $S_{\hat{y}}$. The SD value was then calculated by the formula

$$\text{SD} = \sqrt{S_{\hat{x}}^2 + S_{\hat{y}}^2}.$$

The SD value is invariant under rotation, and $0 \leqslant \text{SD} \leqslant 1$. Computer simulations with 10–10,000,000 random vectors gave SDs $\geqslant 0.95$.

Randomness of vector direction was also evaluated by a chi square test. It was assumed that if a particle can move in any direction, the probability that a particle's mean direction (V) could be anywhere in the range of 0–360 degrees was uniform. For each cell in which N particles were evaluated, we divided a circle into equal-sized sectors described by $360/N$ degrees each. The number of particles in each sector was counted and the chi-square statistic calculated by the following formula:

$$\chi^2 = \sum_{i=1}^{N} (O_i - E_i)^2/E_i,$$

where N was the number of sectors for a given cell, O_i the number of particles observed in the i^{th} sector, and E_i the expected number of particles in the i^{th} sector. A null hypothesis of no significant deviation from randomness was accepted if the test statistic (with $N - 1$ degrees of freedom) did not exceed tabulated values at the $P = 0.05$ level of certainty.

Electron Microscopy

Amebae were fixed in glutaraldehyde and formaldehyde, postfixed with osmium tetroxide, and stained with uranyl acetate and lead citrate by standard methods (Hayat, 1989). Embedded samples were sectioned with a Reichert Ultracut E ultramicrotome and examined in a Zeiss EM10A electron microscope.

Results

Cellular Motility and Shape

Although cellular velocity, morphometric changes, and intracellular particle movement before and immediately after cAMP addition were characterized in detail in a preceding study of *D. discoideum* strain AX3 (Wessels et al., 1989), the analysis had to be repeated on *D. discoideum* strain AX4, the parent strain of the myosin II heavy chain null mutant HS2215, since it was previously demonstrated that normal AX4 cells translocated at half the velocity of AX3 cells (Wessels et al., 1988). 30 aggregation-competent amebae of strain AX4 (W.T.) were examined. 25 of the 30 amebae were elongate, moved in a relatively polar fashion, and formed pseudopodia predominantly at the anterior end when perfused with buffer (Fig. 1, *A–D*). 5 of the 30 amebae did not actively translocate during the period of analysis. Expansion zones, computer generated in difference pictures (see Materials and Methods), formed predominantly at the leading end of each of 5 motile cells analyzed quantitatively with DMS (Fig. 2, *W.T., A–E*). When pulsed with 10^{-6} M cAMP, cellular translocation was suppressed within seconds in the 25 translocating amebae. In the representative centroid track in Fig. 3 *A*, persistent cellular translocation was evident before cAMP addition (−20–0 s), but was lost 2–4 s after cAMP addition. The shape of each of the five DMS-analyzed AX4 amebae remained relatively fixed between 0 and 8 s after

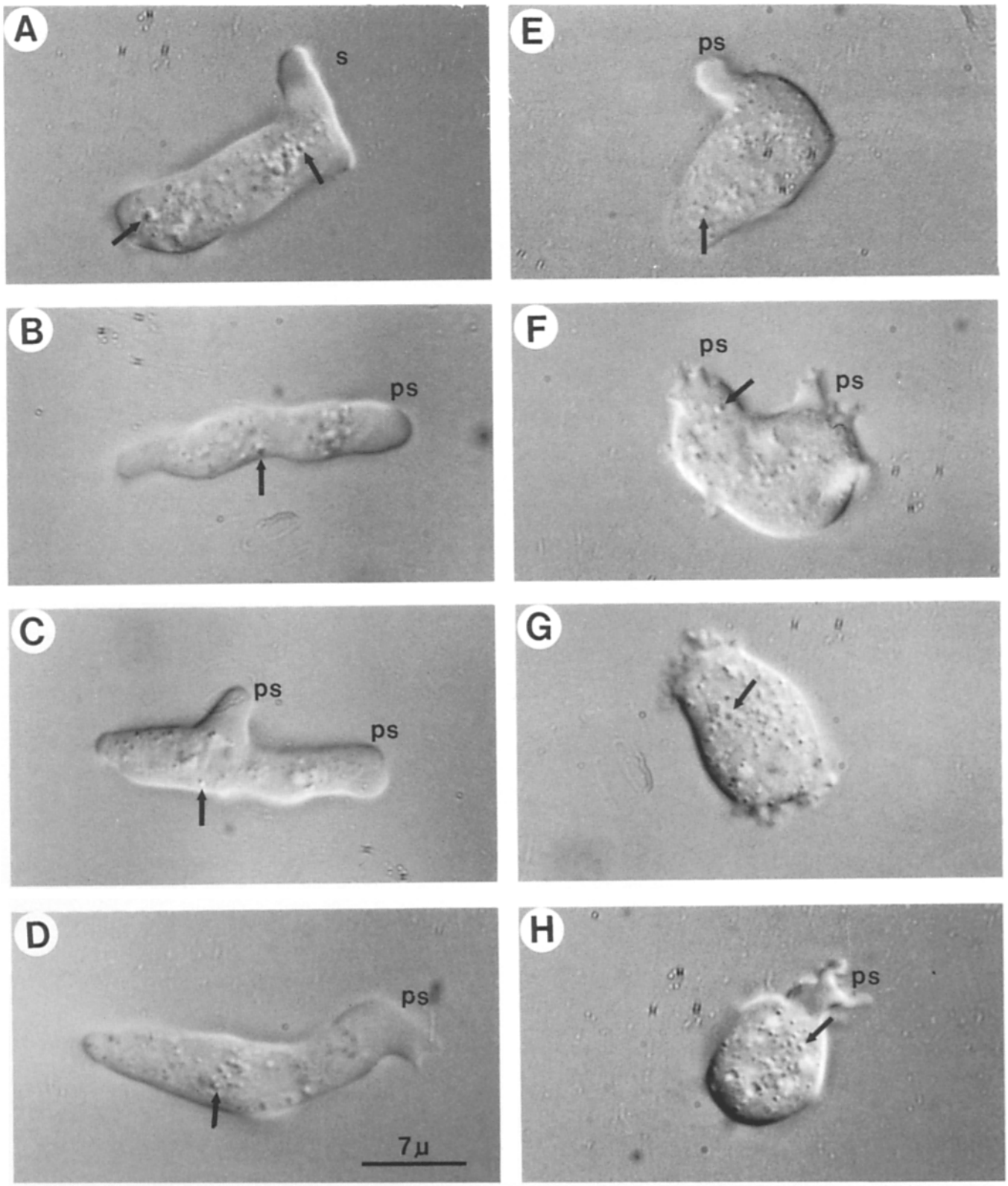

Figure 1. Differential interference contract (DIC) micrographs of wild-type (W.T.) AX4 amebae (*A–D*) and myosin II null mutant HS2215 amebae (*E–H*). Cells from developmental cultures at the onset of aggregation (7 h for W.T. and 9 h for HS2215) were inoculated into a Dvorak-Stotler chamber and perfused with buffered solution. Note the elongate shapes of W.T. cells and the rounder shapes of HS2215 cells. Note also the difference in the shapes of particle free pseudopodia (*ps*) in the two strains. Arrows point to the types of intracellular particles analyzed.

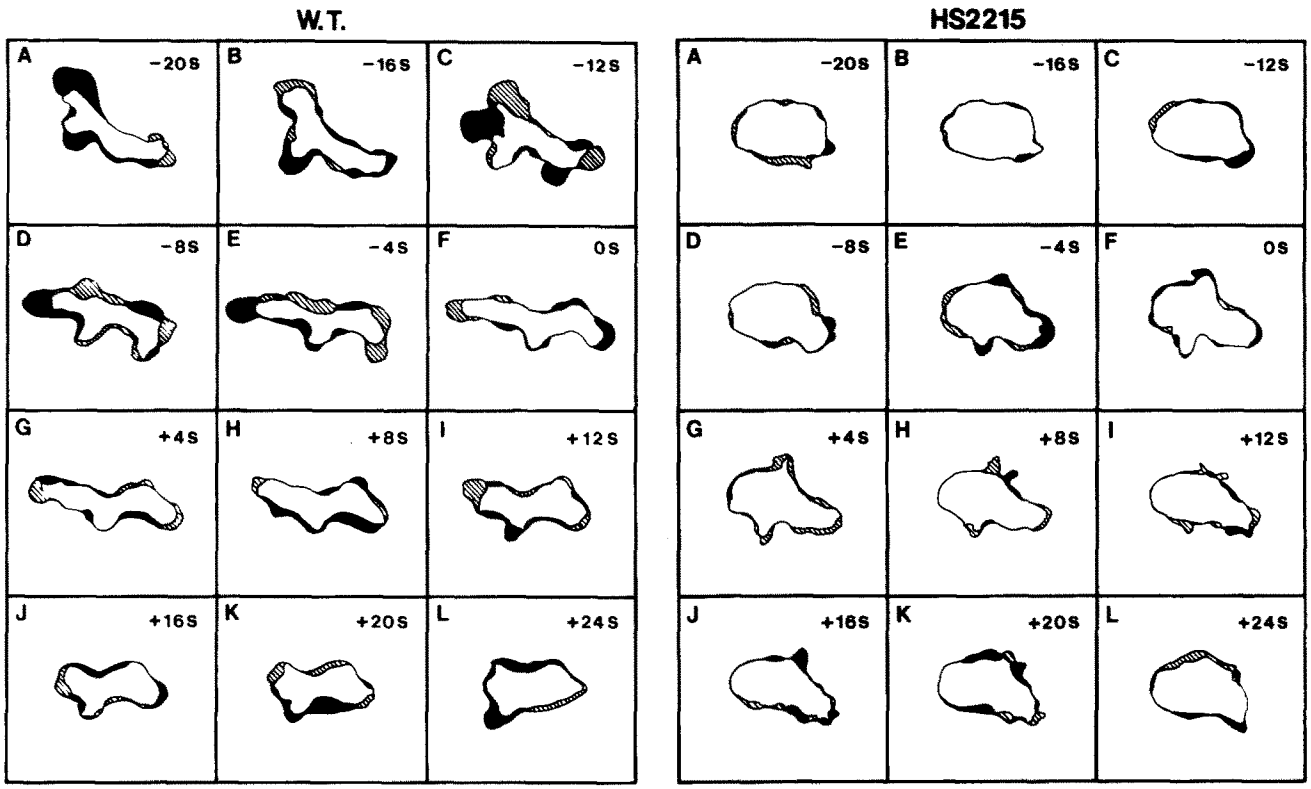

Figure 2. "Difference pictures" of a representative AX4 ameba (W.T.) and a representative HS2215 ameba before and after the addition of cAMP. The difference picture in each panel represents the cell image at the time indicated in the upper right hand corner of the panel superimposed on the image 4 s earlier. Expansion zones are filled, contraction zones hatched, and common zones unfilled. Zero time (*0S*) represents the estimated time, ±1 s, at which 10^{-6} M cAMP was added. *A–F* represent the 20-s period (*−20S–0S*) preceding cAMP addition, and *F–L* the 24-s period (*0S* to *+24S*) after cAMP addition. The time necessary for cAMP to achieve final concentration was 8 s (*0* to *+8S*).

cAMP addition (Fig. 2, *W. T., F–H*); after 8 s, each ameba slowly lost its elongate shape as expansion zones appeared in an apparently random fashion around the cell perimeter (see representative cell in Fig. 2, *W.T., H–L*). The mean velocity of the cell centroid of the five DMS-analyzed AX4 amebae was 0.18 μm/s (± SD 0.10) during the 10-s period immediately preceding cAMP addition (−10–0 s), 0.11 μm/s (± SD 0.05) during the 8-s period (0 to + 8 s) immediately after cAMP addition, and 0.12 μm/s (± SD 0.07) during the subsequent 10-s period (+8 to +18 s). Although average centroid velocity decreased by only 40% immediately after the addition of cAMP, it was clear from the centroid track of each of the five cells (see representative track in Fig. 3 *A*) that centroid movement after the addition of cAMP appeared random and due to slight shape changes rather than to persistent, directional cellular translocation. The average rate of centroid translocation before cAMP addition for AX4 cells was roughly half that observed for the more rapidly translocating AX3 cells (Wessels et al., 1988, 1989). However, the rapid decrease in velocity within 2 s after cAMP addition, the relative freeze in cell shape and expansion activity immediately after cAMP addition, the loss of anterior bias for pseudopod formation after 10 s in 10^{-6} M cAMP, and the average centroid velocity following cAMP addition were similar in AX4 and AX3 amebae (Wessels et al., 1989).

We previously reported that aggregation-competent amebae of the myosin-deficient strains HMM (now called HS2200) and mhcA were less elongate, translocated at a far lower rate, and, when examined in difference picture, exhibited far less apical polarity than W.T. cells (Wessels et al., 1988). These characteristics were also true for 30 HS2215 cells analyzed in a similar manner. HS2215 cells perfused with buffer were, on average, rounder than wild-type cells (Fig. 1, *E–H*) and expansion zones at the perimeter of 5 DMS-analyzed amebae were less extensive and formed in a spatially random, or nonpolar, fashion (difference pictures of a representative cell in buffer are presented in Fig. 2, *HS2215, A–E*). The lack of polarity was also evident in centroid tracks. HS2215 tracks contained few persistent runs, and changes in centroid position appeared to be due to changes in shape rather than to persistent cellular translocation (see representative track in Fig. 3 *B*). When HS2215 cells were pulsed with 10^{-6} M cAMP, no apparent change was evident in the shape or behavior of the 30 cells analyzed qualitatively. In addition, no change was evident in the pattern of the expansion zones (Fig. 2, *HS2215, F–L*), the already round shape (Fig. 2, *HS2215, F–L*), or the centroid translocation tracks (Fig. 3 *B*) of the five DMS-analyzed amebae. The already depressed velocity of centroid translocation was relatively unaffected by addition of 10^{-6} M cAMP. Before the addition of cAMP (−10–0 s), the mean velocity of the five DMS-analyzed HS2215 cells was 0.11 μm/s

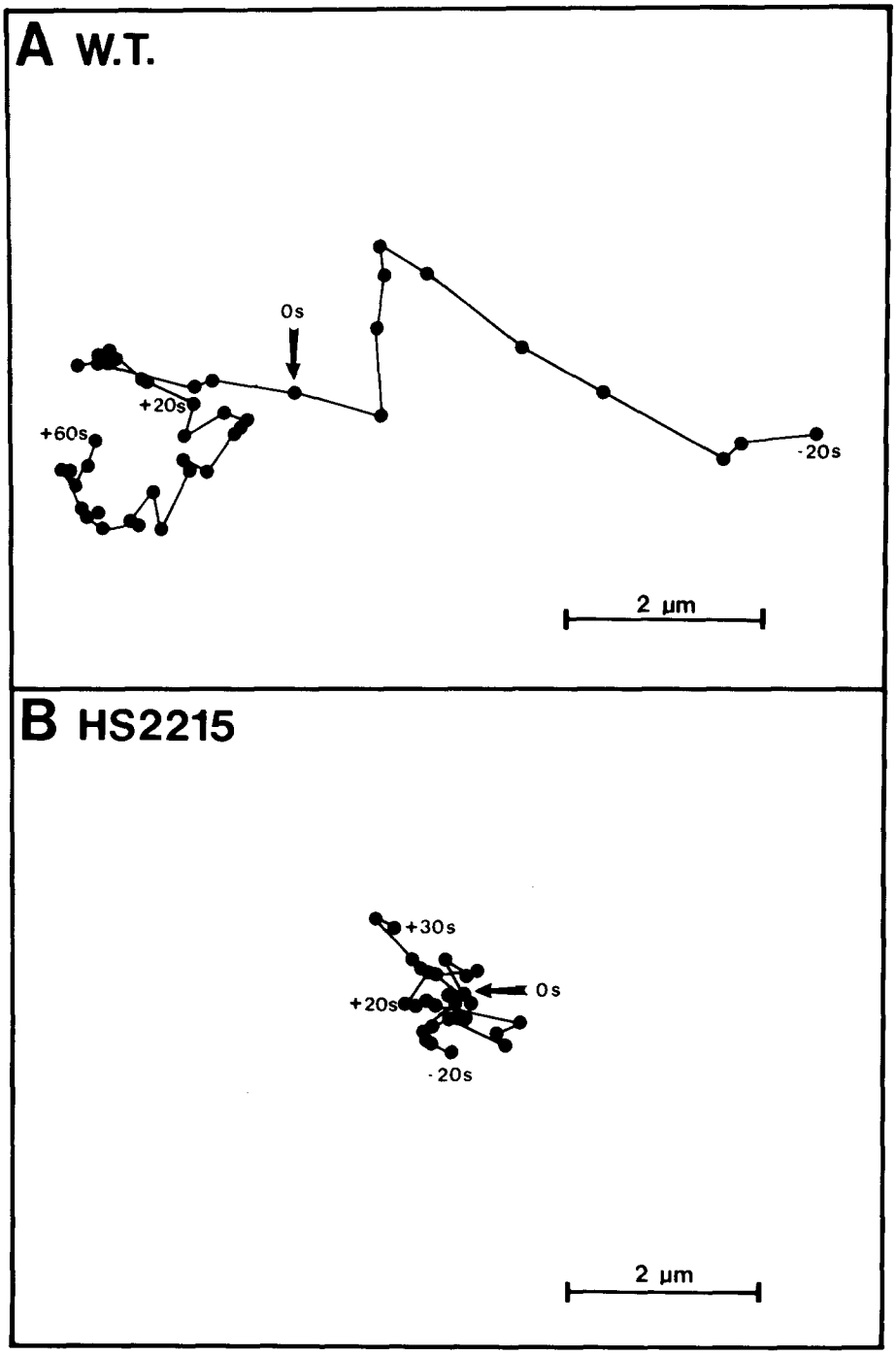

Figure 3. The centroid tracks of a representative AX4 ameba (*A, W.T.*) and a representative HS2215 ameba (*B, HS2215*) before and after cAMP addition. The positions are noted at 2-s intervals. The time at which cAMP first entered the chamber in both cases is noted by an arrow at 0S. The accuracy of this time point was estimated to be ±1 s (Wessels et al., 1989). The centroid translocation tracks between −20S and 0S are for the period before cAMP addition, and the tracks between 0S and +60S, for W.T., and 0S and +30S, for HS2215, are for the periods after cAMP addition. It should be noted that the addition of cAMP to W.T. suppressed subsequent cellular translocation, while cellular translocation was suppressed before and after cAMP addition in the case of HS2215.

(± SD 0.05); immediately after addition (0 to + 8 s), the mean velocity was 0.09 µm/s (± SD 0.03); and between +8 and +18 s, the mean velocity was 0.10 µm/s (± SD 0.03).

Intracellular Particle Velocity

Intracellular particles were visualized with DIC optics (Fig. 1, *A–H*), videorecorded onto 3/4-in tape, and analyzed for velocity and directionality using the SVUI manual digitizing system for DMS (Wessels et al., 1989). When measured in DIC video images (Fig. 1, *A–D*), particle diameters ranged between roughly 0.4 and 1.0 µm. Although the nature of each particle in living cells was not determined at the time of analysis, transmission electron micrographs provided information on the composition of intracellular particles (Fig. 4, *A* and *B*). TEM profiles of intracellular particles in the size range of DIC-visualized particles consisted of approximately half mitochondria and half vesicles in both AX4 and HS2215 cells. The majority of vesicles in this size range in turn contained smaller vesicles or wrapped membranes. These vesicles could not represent food vacuoles with decomposing bacteria since all cells in this study were grown for 2–3 wk in axenic medium and developed to aggregation

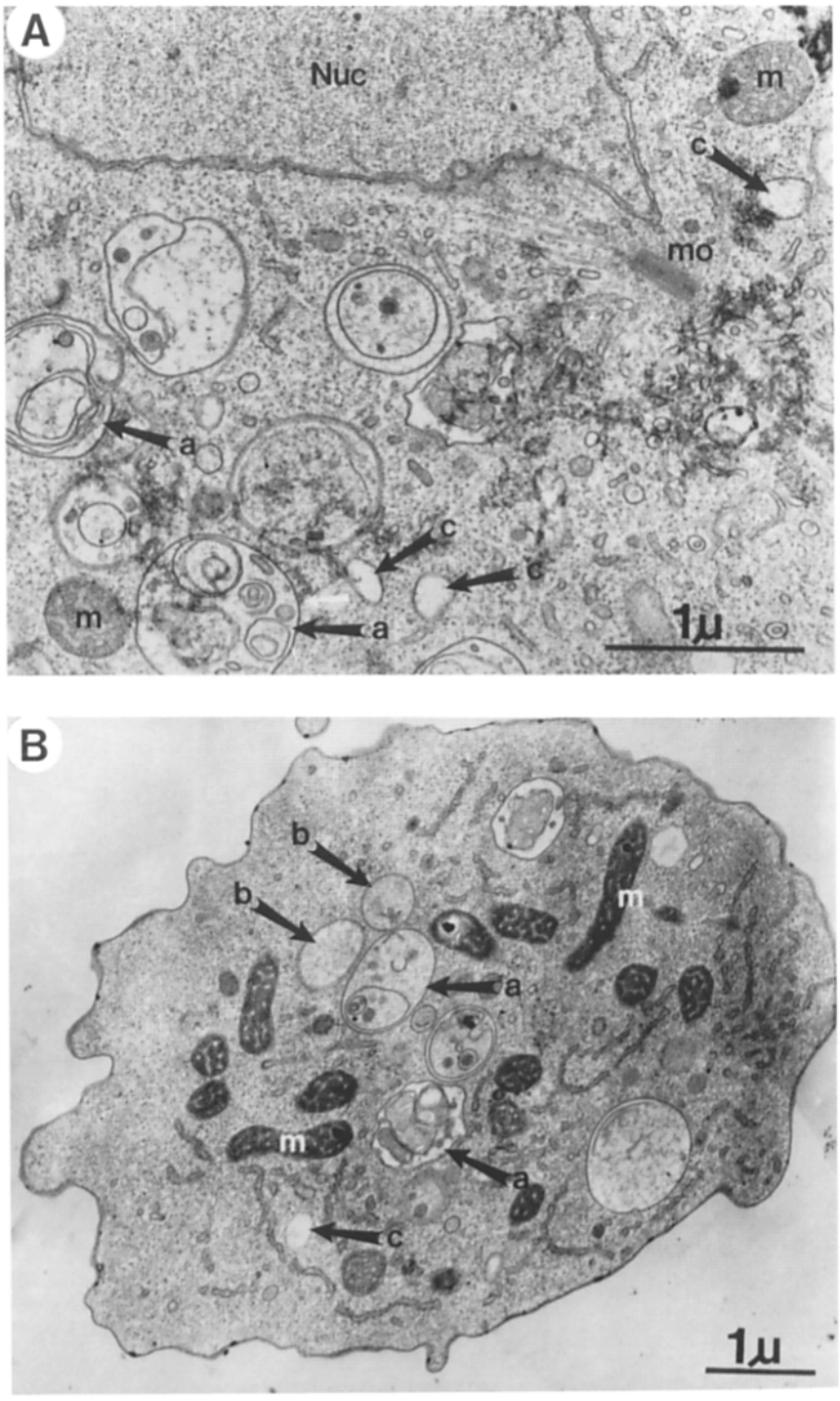

Figure 4. Transmission electron micrographs demonstrating the types of intracellular particles in aggregation competent amebae of *Dictyostelium discoideum*. (*A*) The cytoplasmic region containing a microtubule organizing center, nucleus, vesicles, and mitochondria. (*B*) Lower magnification of a whole cell profile containing mitochondria and membrane bound vesicles. *Nuc*, nucleus; *m*, mitochondria; *mo*, microtubule-organizing body; *a*, membrane-bound vesicles in turn containing smaller membrane bound vesicles or wrapped membranes; *b*, membrane-bound vesicles containing electron-dense material; *c*, small membrane bound vesicles containing electron translucent material.

competency in nonnutrient medium under rigidly sterile conditions (Soll, 1987). Small, sometimes tubular vesicles with diameter below 0.3 μm localized in clusters were below the resolution of the optics used in this study.

Particles moved in and out of the plane of focus for varying lengths of time during the period each cell was videorecorded, and instantaneous velocities (see Materials and Methods for definition) were therefore calculated at 0.5-s intervals during the period of time a particle was in view. All analyzed particles were in view for a minimum of 4 s, and ~20 particles were monitored per cell. In Fig. 5, *A–C*, the instantaneous velocities of individual particles are plotted for three AX4 cells that were actively translocating before the addition of cAMP, and the combined data for the roughly 60 particles analyzed in the three cells are coplotted in *D*. Instantaneous velocities were averaged for each time point and plotted in the lower section of panels for the 3 individual cells (Fig. 5, *A–C*) as well as for the coplotted data (*D*). When AX4 cells were perfused with buffered salts solution (−10 to 0 s), there was a broad distribution of particle velocities, from 0 to 3 μm/second. The mean velocity was 0.71 μm/s (± SD 0.07), exactly half the mean velocity of particles in polarized cells

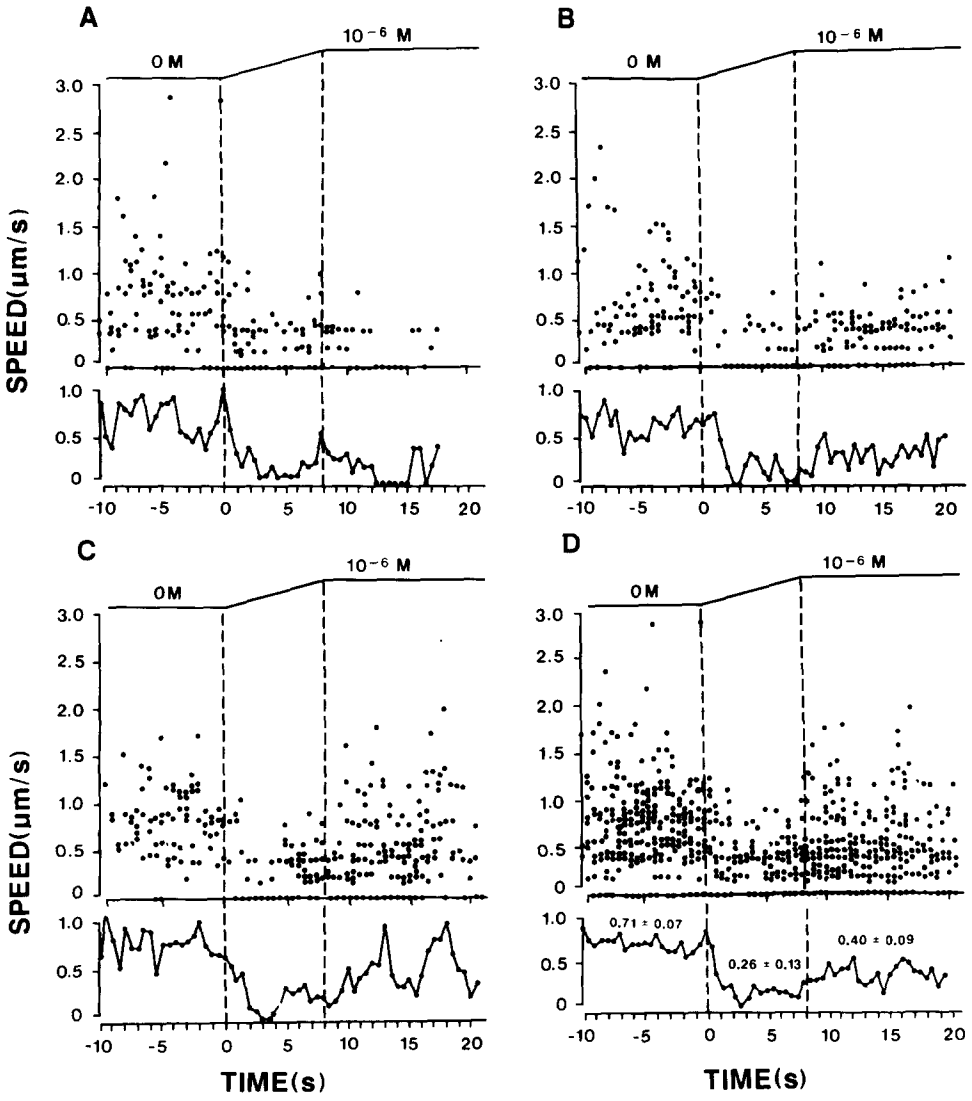

Figure 5. The velocities of intracellular particles in AX4 amebae before and after the addition of 10^{-6} M cAMP. The upper portions of *A*, *B*, and *C* represent measurements of the instantaneous velocities of particles for three individual ameba. The upper portion of *D* is a composite plot of the instantaneous velocities of particles in the three amebae in *A*, *B*, and *C*. The estimated concentration of cAMP in the chamber is presented above each plot. The lower portion of each panel represents the data averaged at each time point. The mean velocities (±SD) for the composite data between −20 and 0 s, 0 and +8 s, and +8 and +18 s are presented in the lower portion of *D*.

of the more rapidly translocating strain AX3 (Wessels et al., 1989). When AX4 cells were pulsed with 10^{-6} M cAMP, there was an abrupt reduction of average particle velocity within 2 s after cAMP first entered the chamber, and a concomitant increase in the proportion of particles exhibiting no detectable movement (0 μm/s) (Fig. 5, *A–C*). This was true for each of the three cells in Fig. 5 and the same dynamics were apparent in each of the 22 additional cells analyzed qualitatively. Approximately 8 s after cAMP first entered the chamber and coinciding with the time cAMP achieved maximum concentration, there was an incomplete rebound in the average velocity of particles. This is best observed in Fig. 6 (*filled circles*) in which the averaged combined data for the three cells in the lower portion of Fig. 5 *D* are smoothed five times using a Tukey window of size 5 with weights of 5, 20, 50, 20, and 5% (Tukey, 1977). In the smoothed plot, there are indications of oscillations with peaks at 11, 16, and 24 s. Although the average velocity of particle movement in AX4 cells before cAMP addition was roughly half that of AX3 cells (Wessels et al., 1989), the average velocity between 0 and 8 s after cAMP addition was identical in the two strains (Wessels et al., 1989).

In Fig. 7, *A–C*, the instantaneous velocities of individual particles are plotted for each of 3 HS2215 cells, and the combined data for ~60 particles analyzed in the three cells are coplotted in *D*. When compared with AX4 cells in buffer (−10 to 0 s), the distribution of particle velocities for HS2215 cells perfused with buffer was depressed, with far more particles exhibiting no measurable velocity. In contrast to the mean particle velocity of 0.71 μm/s (± SD 0.07) for AX4 cells, the mean particle velocity for HS2215 cells was 0.25 μm/s (± SD 0.04), roughly the same mean velocity of AX4 particles (and AX3 particles; Wessels et al., 1989) immediately after the addition of cAMP (Fig. 5 *D*). When HS2215 cells were pulsed with 10^{-6} M cAMP, there was no obvious change in the distribution of particle velocities for the three cells in Fig. 7 nor in the behavior of particles in the 22 additional cells examined qualitatively. Immediately after the addition of cAMP (0–8 s), the mean particle velocity for the combined data of the three cells in Fig. 7 was 0.24 μm/s (± SD 0.05), very close to 0.25 μm/s, the mean velocity before cAMP addition (Fig. 7 *D*). When the averaged combined data (lower portion of Fig. 7 *D*) were smoothed, it was apparent that average particle velocity in HS2215 cells before as well as after cAMP addition was at the low level observed in AX4 cells immediately after cAMP addition

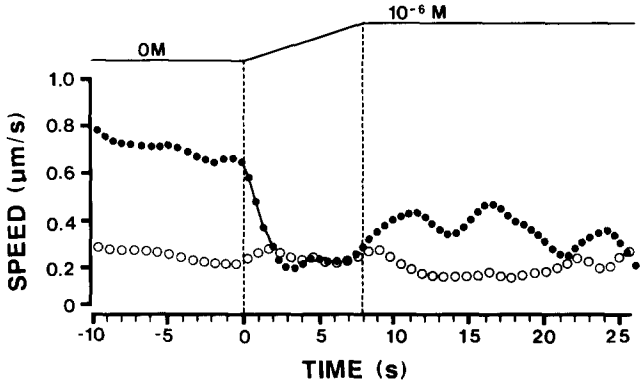

Figure 6. Smoothed data of particle velocities for AX4 (●) and HS2215 (○) amebae. The averaged data of the composite plots of vesicle velocities in Fig. 5 *D* for AX4 cells, and Fig. 7 *D* for HS2215 cells were smoothed 5 times with a Tukey window of size 5 with weights of 5, 20, 50, 20, and 5% (Tukey, 1977).

(Fig. 6). Therefore, in contrast to AX4 cells, cAMP had no measurable effect on the already depressed average velocity of particles in HS2215 cells.

Directionality of Particle Movement

In AX3 cells perfused with buffered salts solution, the majority of rapidly moving intracellular particles exhibited a strong directional bias toward the anterior pseudopod of a translocating cell (Wessels et al., 1989). In Fig. 8, the directions of particles in five normal cells are plotted in relation to the direction of cellular translocation assessed prior to cAMP addition. At the left end of each panel, the directions of cellular translocation at −10 and −1 s before the addition of cAMP are demarcated at the ends of the dashed curve, and the average direction during this period, noted by an arrow, is equated with 0°. The track of each particle has been converted to a straight vector, and the direction of each vector calculated according to the formula in Materials and Methods. Vector directions could range from 0°, the average direction of cellular translocation before cAMP addition, to 180°, opposite to the average direction of cellular translocation. In each vector plot, a dashed vertical line demarcates 90° and separates vector directions into anterior (0–90°) and posterior (90–180°). The length of each vector is equal to net distance in vector direction divided by the time the particle was tracked. The origins of all vectors are positioned at a common point. Therefore, each vector points in the average direction of particle translocation and the length of each vector is proportional to particle speed.

Vector plots *a* in each panel in Fig. 8 represent particles of AX4 cells monitored between −10 and 0 s, before 10^{-6} M cAMP addition, and vector plots *b* represent particles monitored between +8 and +18 s after cAMP addition, during the partial rebound in particle velocity. Before the addi-

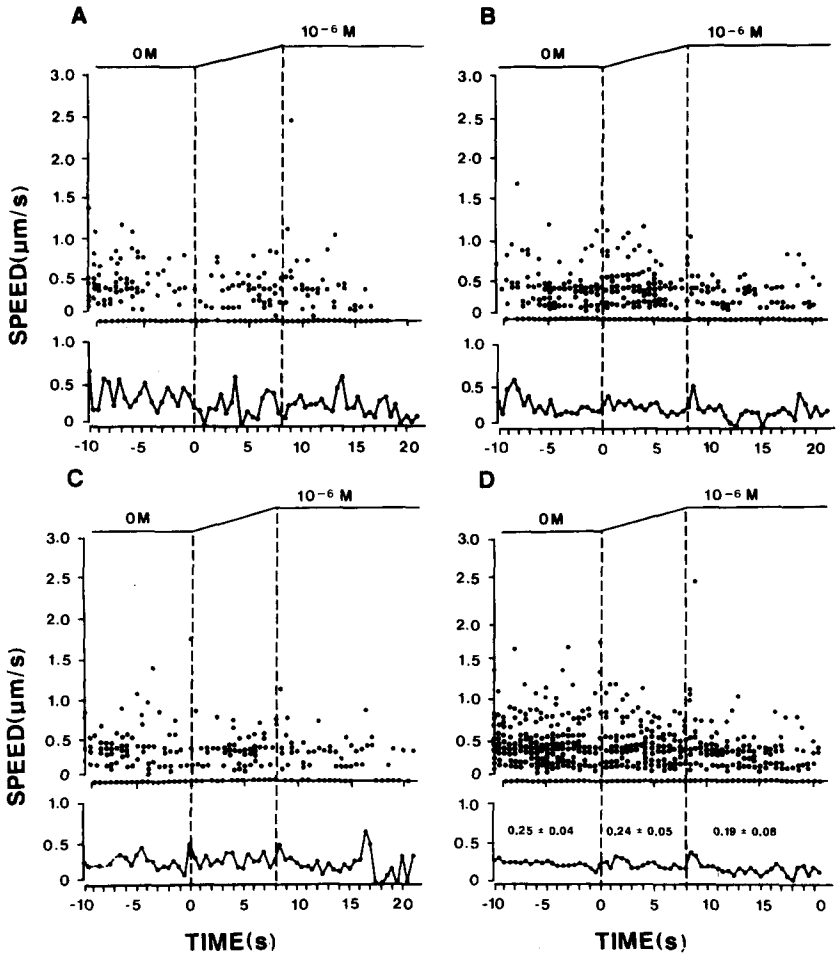

Figure 7. The velocities of particles in HS2215 amebae before and after the addition of 10^{-6} M cAMP. The explanation for this figure is identical to the one presented in the legend to Fig. 5 for AX4 cells.

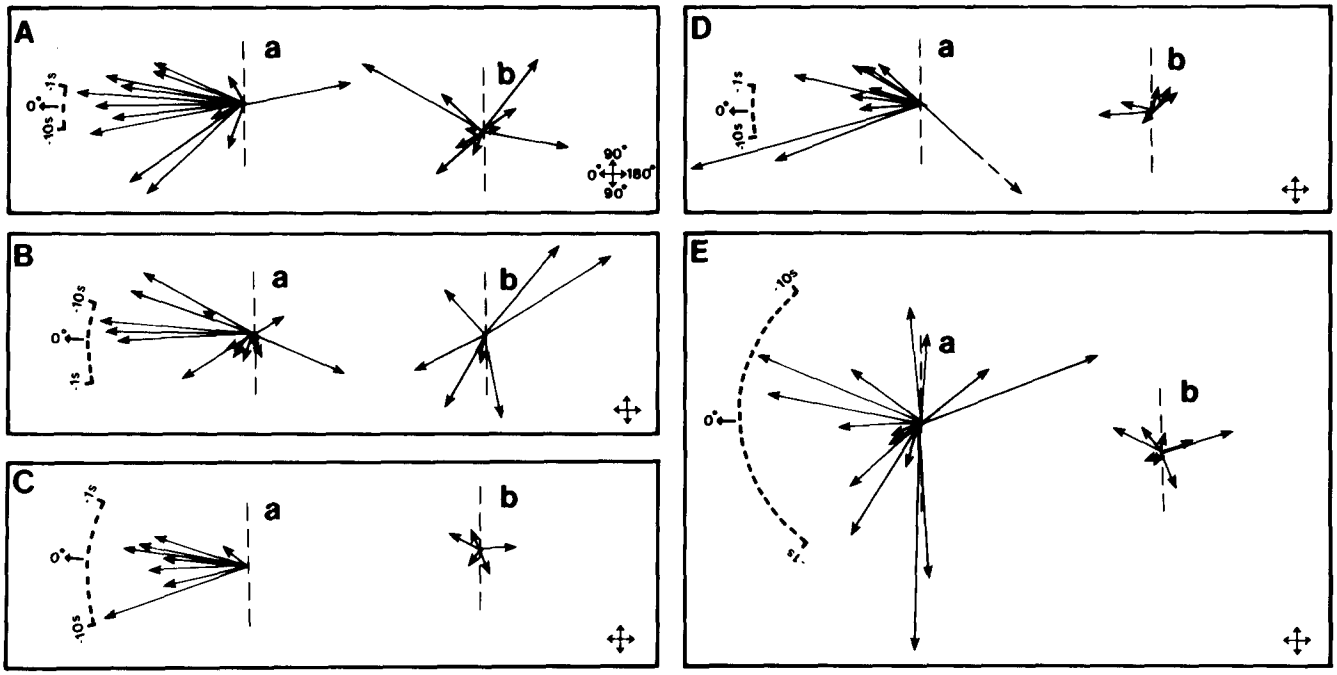

Figure 8. The direction of particles in AX4 cells (*A–E*) before (−10 to 0 s) the addition of cAMP (*a*) and after (+8 to +18 s) the addition of cAMP (*b*). The track of each particle has been converted to a vector. The length of the vector is equal to net distance in direction divided by the time of particle tracking, and the direction of each vector reflects the average direction of the particle in relation to the direction of cellular translocation. The origins of all vectors monitored in a single cell are positioned at a single point. The direction of cellular translocation prior to cAMP addition is diagrammed for each cell to the left of the panel, the directions at −10 and at −1 s before cAMP addition demarcating the ends of a dashed curve and the average direction noted by an arrow at 0°. A vertical dashed line is drawn through the vector origin to separate anterior (0–90°) from posterior (90–180°).

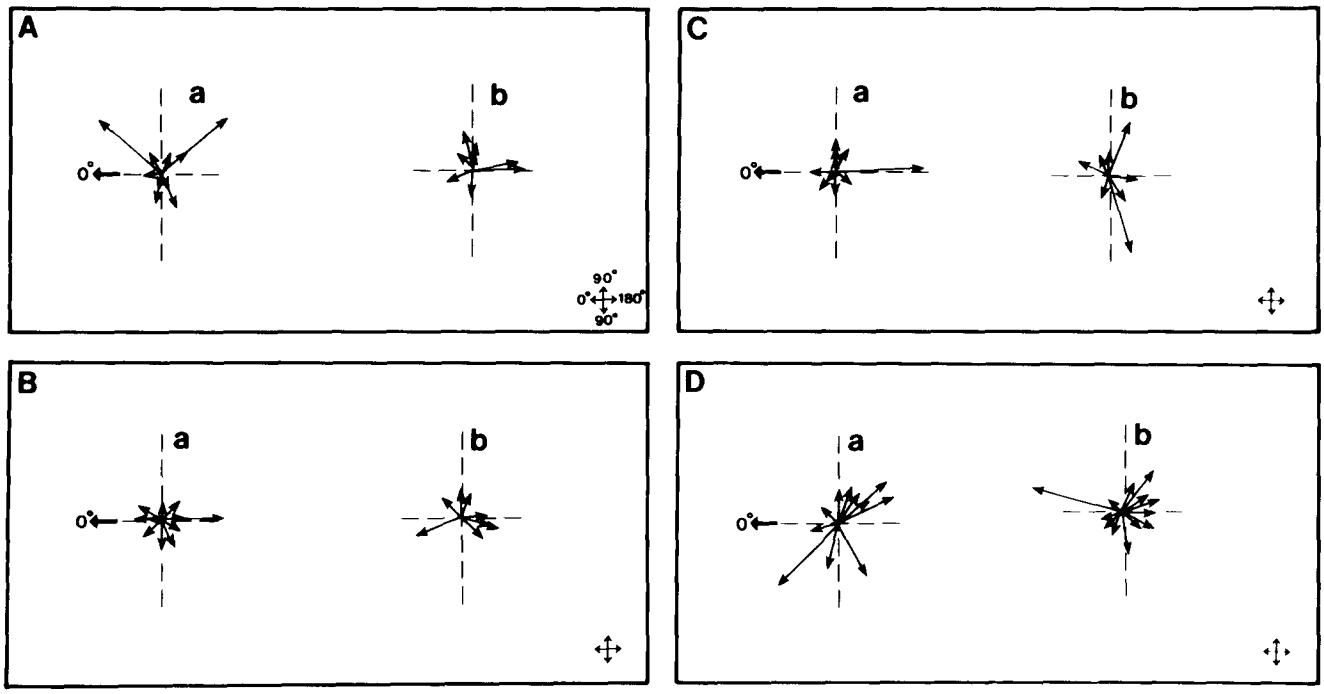

Figure 9. The direction of particles in HS2215 cells (*A–D*) before (−10 to 0 s) the addition of cAMP (*a*) and after (+8 to +18 s) the addition of cAMP (*b*). The arrow pointing to 0° to the left of each panel represents the average direction of centroid translocation between −10 and −1 s before cAMP addition. The directions at −10 and −1 s are not presented at the ends of a dashed curve, as in the case of AX4 cells in Fig. 8, since HS2215 cells did not exhibit persistent centroid translocation in a given direction. A vertical dashed line is drawn through the vector origins to separate "anterior" (0–90°) from "posterior" (90–180°), and a horizontal dashed line is drawn to separate "right" from "left."

Table I. An Evaluation of Particle Direction in AX4 and HS2215 Cells

		Pre-cAMP (−10 to 0 s)		Post-cAMP (+8 to +18 s)	
	Cell	SD	*P* value	SD	*P* value
AX4	A	0.70	<0.005	0.99	NS
	B	0.87	<0.025	0.95	<0.05
	C	0.27	<0.0001	0.99	NS
	D	0.65	<0.025	0.95	NS
	E	0.93	NS	0.99	NS
Average SD		0.68		0.97	
HS2215	A	0.98	NS	0.97	NS
	B	0.98	NS	0.93	NS
	C	0.98	NS	1.00	NS
	D	0.97	NS	0.99	NS
Average SD		0.98		0.97	

The standard deviation of vector direction (SD), and the *P* value for randomness by the chi square test were calculated as described in Materials and Methods. The lower threshold for randomness was a standard deviation of 0.95, and, for the chi square test, a *P* value of 0.05. A *P* value of 0.05 or greater was considered not significant (NS). Note that the one AX4 cell (cell E) exhibiting a SD close to 0.95 and a *P* value of 0.05 or greater was turning during the analysis (see *E* in Fig. 8).

tion of cAMP, the majority of particles in the 5 AX4 cells moved rapidly, and, in most cases, in the general direction of cellular translocation (Fig. 8, *A–D*). Of the 62 particles monitored within −10 to 0 s in the five cells, 52 (84%) were directed anteriorly, while 10 (16%) were directed posteriorly. The cell in Fig. 8 *E* made a wide turn (note the extent of the arc between *−10s* and *1s*), but even in this case, 11 of the 14 particles moved towards the edge of the anterior hemisphere of the cell. Between +8 and +18 s after the addition of 10^{-6} M cAMP, rebounding particles in all five cells exhibited prolonged tracks, but they no longer exhibited the strong directional bias towards the original anterior end of the cell. Of the 38 particles monitored between +8 and +18 s in the five cells, 21 (55%) moved in the original anterior direction and 17 (45%) moved in the posterior direction. These results demonstrate that after addition of cAMP to rapidly translocating AX4 cells, particle movement loses the original anterior bias. Similar particle behavior was observed in 20 additional translocating AX4 amebae examined qualitatively, and was previously reported for AX3 amebae (Wessels et al., 1989).

In Fig. 9, vector plots are presented for particles in 4 HS2215 cells between −10 and 0 s preceding cAMP addition (vector plots *a*), and between +8 and +18 s after cAMP addition (vector plots *b*). Although translocation of the 4 HS2215 cells exhibited no persistent directionality, as in the case of AX4 cells, 0° to the left of each panel represents the average direction of cellular (centroid) translocation between −10 and −1 s before cAMP addition, and a vertical dashed line is drawn at 90° to demarcate anterior and posterior directions. Before cAMP addition, particles appeared to exhibit no strong directional bias. Of the 43 particles monitored within −10 and 0 s in the four cells, 20 (47%) moved anteriorly and 23 (53%) moved posteriorly. After cAMP addition, particles continued to exhibit the same absence of a preferred direction. Of the 38 particles monitored within +8 and +18 s in the 4 cells, 16 (42%) moved "anteriorly" and 22 (58%) moved "posteriorly." Since anterior (0°) in the case of HS2215 cells is basically arbitrary, we also compared arbitrary right- and left-directed particles for possible bias. Before cAMP addition, 52% were directed to the right and 48% to the left; after cAMP addition, 53% were directed to the right and 47% to the left. Apparently random particle direction before and after cAMP addition was observed in 26 additional HS2215 examined qualitatively.

To assess more rigorously the degree of randomness of particle paths in each cell, we measured the standard deviation (SD) of particle vector direction (see Materials and Methods). An SD of 0.0 represents a single direction for all particle vectors, and an SD of 1.0 represents a uniformly random distribution in a single cell. Computer simulations of up to 10^6 vectors with random direction resulted in a lower threshold SD of 0.95 for randomness (see Materials and Methods). The SD of vector directions for the five AX4 cells in Fig. 8 and for the four HS2215 cells in Fig. 9 are presented in Table I. Before the addition of cAMP (−10 to 0 s), four of the five AX4 cells exhibited relatively low SD values ranging from 0.27 to 0.87. The one AX4 cell exhibiting a relatively high SD of 0.93 (cell *E* in Fig. 8) was turning at the time of analysis. The mean SD for the five AX4 cells before cAMP addition was 0.68. During the rebound period after cAMP addition (+8 to +18 s), the SD values for all of the five cells were ≥0.95, and the mean SD was 0.97. The SD values of particle vector directions for the four HS2215 before cAMP addition (−10 to 0 s) were 0.97, and averaged 0.98. After the addition of cAMP (+8 to +18 s), the SD values ranged between 0.93 and 1.00 with a mean of 0.97. Therefore, vector directions were assessed as nonrandom by this method only in four of the five AX4 cells before cAMP addition.

We also evaluated randomness by applying a chi square test. We divided the encompassing area in which particles moved in equally sized sectors described by an arc of $360°/N$, where N was the number of particles (see Materials and Methods). A null hypothesis of no significant deviation from randomness was accepted if the test statistic (with $N-1$ degrees of freedom) did not exceed tabulated values at the $P = 0.05$ level of certainty. Before cAMP addition, four of the five AX4 cells exhibited a *P* value <0.05. After cAMP addition, only one of the five AX4 cells exhibited a *P* value <0.05. None of the HS2215 cells exhibited a *P* value <0.05. Again, this analysis supports the conclusion that particle direction is nonrandom only in AX4 amebae rapidly translocating in buffer.

Discussion

Myosin II has been demonstrated by indirect immunofluorescence to be localized in the posterior two-thirds of motile *Dictyostelium* amebae (Yumura and Fukui, 1985). This localization is consistent with previous suggestions that myosin-based contraction in the posterior portion of a translocating cell supplies the active force for anterior pseudopod expansion (Taylor and Fechheimer, 1982; Fukui and Yumura, 1986; Spudich, 1989). It was therefore surprising to discover that when myosin II was selectively removed from *Dictyostelium* by either insertional mutagenesis in the case

of the recombinant HMM (De Lozanne and Spudich, 1987) or by transformation with an antisense construct in the case of strain mhcA (Knecht and Loomis, 1987), the amebae were still able to translocate (De Lozanne and Spudich, 1987; Knecht and Loomis, 1987), form F-actin-filled pseudopodia (Wessels et al., 1988), exhibit a chemotactic response (Peters et al., 1988; Wessels et al., 1988), rapidly accumulate actin in the Triton-insoluble cytoskeletal fraction after cAMP stimulation (Peters et al., 1988), and accumulate cGMP and cAMP in response to cAMP stimulation (Peters et al., 1988). However, when the motile behaviors of these myosin II–deficient strains were analyzed in detail with the computer-assisted Dynamic Morphology System (Soll, 1988; Soll et al., 1988), it was discovered that the rate of cellular translocation, pseudopod formation, anterior polarity, and morphology were aberrant (Wessels et al., 1988).

Here, we have examined the role of myosin II in intracellular particle behavior. Using videorecordings of DIC images, intracellular particles were tracked in 30 AX4 and 30 HS2215 amebae and analyzed either qualitatively, or quantitatively with a newly developed manual digitizing system for DMS (Wessels et al., 1989). Although the identity of each particle analyzed from DIC images was not known, electron micrographs indicated that within the size range of DIC-analyzed particles (0.4–1.0 μm diameters), there were roughly the same proportions of membrane-bound vesicles and mitochondria in cells of both the normal parent strain AX4 and the myosin II null mutant HS2215 (Manstein et al., 1989). The DIC-analyzed particles did not include small, usually clustered vesicles with diameters of <0.3 μm.

HS2215 amebae exhibit abnormal intracellular particle behavior. The average velocity of intracellular particles in HS2215 amebae perfused with buffer was approximately one-third that in AX4 amebae. In addition, there were far more immobile particles and far fewer particles with velocities >1.0 μm/s. Depressed particle velocity in HS2215 amebae perfused with buffer was similar to that observed in parent AX4 cells (and AX3 cells; Wessels et al., 1989) immediately after the addition of 10^{-6} M cAMP, suggesting that rapid saltatory particle movement, which is depressed by the addition of cAMP, requires myosin II. This conclusion is supported by the observation that the addition of 10^{-6} M cAMP had no further effect on the already depressed behavior of intracellular particles in HS2215 cells.

In addition to a depression in particle velocity and the absence of a cAMP effect, the absence of myosin II resulted in the loss of the anterior bias observed in the paths of particles in AX4 cells. Tracks of particles in HS2215 cells exhibited no preferred direction when examined qualitatively and quantitatively, and this correlated with the absence of directional bias in pseudopod expansion. It is tempting to suggest from these results that directed vesicle movement towards the anterior of a translocating cell is involved in membrane insertion for the anteriorly expanding pseudopod (Singer and Kupfer, 1986), and that this process is dependent upon myosin II. However, it is not clear whether (*a*) the absence of directional bias in particle movement in HS2215 cells results in a loss of directional bias in pseudopod expansion, (*b*) the absence of directional bias in pseudopod expansions results in the absence of bias in particle movement, or (*c*) both are parallel, independent effects due to the absence of myosin II.

The results presented here for strain HS2215 and in a previous study for strains HMM and mhcA (Wessels et al., 1988) demonstrate that the absence of myosin II affects (*a*) cell shape, (*b*) the polarity and dynamics of pseudopodial expansion, (*c*) cellular velocity, (*d*) intracellular particle velocity, (*e*) intracellular particle directionality, and (*f*) the rapid inhibition of intracellular particle movement by 10^{-6} M cAMP. It has been demonstrated that the addition of cAMP to cultures of suspended amebae causes rapid changes in the association of myosin II heavy chain and the Triton-insoluble cytoskeleton (Liu and Newell, 1988; Dharmwardhane et al., 1989) and the phosphorylation of myosin II heavy chain (Malchow et al., 1981; Berlot et al., 1987), and the addition of cAMP to amebae overlayed with agarose results in changes in the localization of myosin II–containing rods in the endoplasm and cortex (Yumura and Fukui, 1985). These changes are very likely related to the cAMP-stimulated changes in cell motility, cell shape, and polarity, and intracellular particle movement that we have demonstrated are present in normal AX4 amebae, but absent in amebae lacking myosin II heavy chain. However, our results do not demonstrate whether myosin II is directly involved in these cellular processes, or whether it plays a role indirectly by maintaining the general integrity of the cytoskeleton, a possibility suggested by Spudich in a recent review of myosin II function (Spudich, 1989). What seems remarkable is that the removal of a single actin-based motor molecule can exert such a pleiotropic effect on so many cellular parameters related to the normal motile behavior of a chemotactically responsive ameba.

We are heavily indebted to Dr. James Spudich and colleagues for generously providing us with the HS2215 and parent AX4 strains for analysis. We are grateful to Dr. Ed Voss for the computer programming, Dr. D. Jackola for help with statistical analysis, and to C. Bucheit, D. Kruse, H. Vawter, and F. Rogness for help in developing the figures and assembling the manuscript.

This project was funded by grants HD18577 and GM2583 from the National Institutes of Health and by a grant from the Iowa Development Commission for the development of the SVUI Manual Digitizer and customized DMS programs.

Received for publication 5 February 1990 and in revised form 11 May 1990.

References

Berlot, C. H., P. N. Devreotes, and J. A. Spudich. 1987. Chemoattractant-elicited increases in *Dictyostelium* myosin phosphorylation are due to changes in myosin localization and increases in kinase activity. *J. Biol. Chem.* 262:3918–3926.

Cocucci, S., and M. Sussman. 1970. RNA in cytoplasmic and nuclear fractions of cellular slime mold amebae. *J. Cell Biol.* 45:399–407.

De Lozanne, A., and J. A. Spudich. 1987. Disruption of the *Dictyostelium* myosin heavy chain gene by homologous recombination. *Science (Wash. DC).* 236:1086–1091.

Dharmwardhane, S., V. Warren, A. Hall, and J. Condeelis. 1989. Changes in the association of actin-binding proteins with the actin cytoskeleton during chemotactic stimulation of *Dictyostelium discoideum. Cell Motil. Cytoskel.* 13:57–63.

Fukui, Y., and S. Yumura. 1986. Actomyosin dynamics in chemotactic amoeboid movement of *Dictyostelium. Cell Motil. Cytoskel.* 6:662–673.

Hayat, M. A. 1989. Principles and Techniques of Electron Microscopy: Biological Applications. CRC Press, Inc., Boca Raton, FL.

Knecht, D. A., and W. F. Loomis. 1987. Antisense RNA inactivation of myosin heavy chain gene expression in *Dictyostelium discoideum. Science (Wash. DC).* 236:1081–1091.

Liu, G., and P. C. Newell. 1988. Evidence that cyclic GMP regulates myosin interaction with the cytoskeleton during chemotaxis of *Dictyostelium. J. Cell Sci.* 90:123–129.

Malchow, D., R. Bohme, and H. J. Rahmsdorf. 1981. Regulation of phosphorylation of myosin heavy chain during the chemotactic response of *Dictyostelium* cells. *Eur. J. Biochem.* 117:213–218.

Manstein, D. J., M. A. Titus, A. De Lozanne, and J. Spudich. 1989. Gene replacement in *Dictyostelium*: generation of myosin null mutants. *EMBO (Eur. Mol. Biol. Organ.) J.* 8:923–932.

Ogihara, S., J. Carboni, and J. Condeelis. 1988. Electron microscopic localization of myosin II and ABP-120 in the cortical actin matrix of *Dictyostelium* amebae using IgG-gold conjugates. *Dev. Genet.* 9:505–520.

Peters, D., D. A. Knecht, W. F. Loomis, A. De Lozanne, J. Spudich, and P. J. M. Haastert. 1988. Signal transduction, chemotaxis, and cell aggregation in *Dictyostelium discoideum* cells without myosin heavy chain. *Dev. Biol.* 128:158–163.

Sinard, J. H., and T. D. Pollard. 1989. Microinjection into *Acanthamoeba castellanii* of monoclonal antibodies to myosin II slows but does not stop cell locomotion. *Cell Motil. Cytoskel.* 12:42–52.

Singer, S. J., and A. Kupfer. 1986. The directed migration of eukaryotic cells. *Annu. Rev. Cell Biol.* 2:337–365.

Soll, D. R. 1987. Methods for manipulating and investigating developmental timing in *Dictyostelium discoideum*. *Methods Cell Biol.* 28:413–431.

Soll, D. R. 1988. "DMS," a computer-assisted system for quantitating motility, the dynamics of cytoplasmic flow and pseudopod formation: its application to *Dictyostelium chemotaxis*. *Cell Motil. Cytoskeleton. (Suppl).* 10:91–106.

Soll, D. R., E. Voss, and D. Wessels. 1987. Development and application of the "Dynamic Morphology System" for the analysis of moving amebae. *Proc. SPIE (Soc. Photo-opt. Instr. Eng.).* 832:821–830.

Soll, D. R., E. Voss, B. Varnum-Finney, and D. Wessels. 1988. The "dynamic morphology system": a method for quantitating changes in shape, pseudopod formation and motion in normal and mutant amebae of *Dictyostelium discoideum*. *J. Cell. Biochem.* 37:177–192.

Spudich, J. A. 1989. In pursuit of myosin function. *Cell Reg.* 1:1–11.

Taylor, D. C., and M. Fechheimer. 1982. Cytoplasmic structure and contractility: the solation-contraction coupling hypothesis. *Philos. Trans. R. Soc. Lond. B. Biol. Sci.* 299:185–197.

Tukey, J. W. 1977. Exploratory Data Analysis. Addison-Wesley Publishing Co., Reading, MA.

Varnum, B., and D. R. Soll. 1984. Effects of cAMP on single cell motility in *Dictyostelium*. *J. Cell Biol.* 99:1151–1155.

Wessels, D., D. R. Soll, D. Knecht, W. F. Loomis, A. DeLozanne, and J. Spudich. 1988. Cell motility and chemotaxis in *Dictyostelium* amebae lacking myosin heavy chain. *Dev. Biol.* 128:164–177.

Wessels, D., N. A. Schroeder, E. Voss, A. L. Hall, J. Condeelis, and D. R. Soll. 1989. cAMP-mediated inhibition of intracellular particle movement and actin reorganization in *Dictyostelium*. *J. Cell Biol.* 109:2841–2851.

Yumura, S., and Y. Fukui. 1985. Reversible cyclic AMP-dependent change in distribution of myosin thick filaments in *Dictyostelium*. *Nature (Lond.).* 314:194–196.